Winter 10-2011

Thickness-shear and Thickness-twist Vibrations of an AT-cut Quartz Mesa Resonator

Huijing He
University of Nebraska-Lincoln, he.hui.jing@hotmail.com

Jinxi Liu
Shijiazhuang Tiedao University

Jiashi Yang
University of Nebraska-Lincoln, jyang1@unl.edu

Thickness-Shear and Thickness-Twist Vibrations of an AT-Cut Quartz Mesa Resonator

Huijing He, Jinxi Liu, and Jiashi Yang

***Abstract*—We study thickness-shear and thickness-twist vibrations of an AT-cut quartz plate mesa resonator with stepped thickness. The equations of anisotropic elasticity are used with the omission of the small elastic constant c_{56}. An analytical solution is obtained using Fourier series from which the resonant frequencies, mode shapes, and energy trapping are calculated and examined. The solution shows that a mesa resonator exhibits strong energy trapping of thickness-shear and thickness-twist modes, and that the trapping is sensitive to some of the structural parameters of the resonator.**

I. Introduction

Piezoelectric crystals are widely used to make resonators, filters, sensors, and other acoustic wave devices for time-keeping, frequency generation and operation, telecommunication, and sensing. Thickness-shear (TSh) vibrations of crystal plates are in common use for these applications [1], [2]. TSh modes can be excited in quartz plates, ceramic plates with in-plane poling, and plates of crystals of class 6mm with in-plane 6-fold axis, etc. Theoretically, TSh modes can only exist in unbounded plates without edge effects. When a plate is vibrating in TSh modes, motions of the material particles of the plate are parallel to the surfaces of the plate, and particle velocities vary along the plate thickness only, without in-plane variations.

In reality, however, because of the finite sizes of devices, pure TSh modes cannot exist because of edge effects. Therefore, in real devices, the actual operating TSh modes have slow in-plane variations. These modes have been referred to as transversely varying TSh modes [3]. In the case in which the in-plane mode variation is along the direction perpendicular to the TSh particle velocity, the modes are called thickness-twist (TT) modes [4], [5].

When a plate is vibrating in TSh modes, every part of the plate is moving except at some planes parallel to the plate surfaces (nodal planes). For such a vibrating plate, mounting (which is necessary for any device) becomes an issue. Fortunately, TSh modes in a plate with partial electrodes (called a trapped energy resonator) have an important and useful behavior called energy trapping, through which the TSh vibration is confined under the electrodes and decays rapidly outside them [6]. Energy trapping is useful in device mounting. For trapped modes, mounting can be done near the plate edges without affecting the vibration of the plate. Energy trapping is mainly due to the inertial effect of the electrodes [6]. Piezoelectric coupling can also contribute to energy trapping [7]. People have also developed contoured resonators [8]–[11] from plates with gradually varying thickness and mesa resonators [12]–[20] from plates with stepped or piecewise constant thickness (see Fig. 1). In contoured or mesa resonators, the changing plate thickness usually leads to energy trapping stronger than the inertia of partial electrodes.

Because of the change of plate thickness, analytical modeling of mesa resonators is mathematically very challenging. Theoretical results are few and scattered. The analysis in [12] was based on approximate, two-dimensional plate equations. In [13]–[20], combined analytical-numerical approach, finite element numerical method, and experimental study were all conducted. Most of [12]–[20] presented results on mode variations along x_1 (the diagonal axis). Only [18] has some results on mode variations along the other in-plane axis x_3. In this paper, we study energy trapping of TSh and TT modes in an AT-cut quartz mesa resonator using the equations of anisotropic elasticity, with a focus on mode variations along x_3. We propose dividing the resonator into several regions, each having a constant thickness for which a Fourier series solution can be constructed with undetermined coefficients. Then solutions of different regions are substituted into the interface continuity conditions among different regions to obtain linear algebraic equations for the undetermined coefficients. In this way, we are able to obtain the solution to the free vibration eigenvalue problem of the resonator, with which we examine the ways in which the resonant frequencies, mode shapes, energy trapping are affected by the thickness change of the mesa resonator.

II. Governing Equations

The equations for anisotropic crystals vary considerably according to crystal symmetry. A particular cut of a crystal plate refers to the orientation of the plate when it is taken out of a bulk crystal. As a consequence, crystal

Manuscript received March 15, 2011; accepted July 17, 2011. This work was supported by the National Nature Science Foundation of China (No. 10972147) and the Program for Changjiang Scholars and Innovative Research Team in University (No. IRT0971).

H. He and J. Liu are with the Department of Engineering Mechanics, Shijiazhuang Tiedao University, Shijiazhuang, China (e-mail: liujx02@hotmail.com).

J. Yang is with the Department of Engineering Mechanics, University of Nebraska, Lincoln, NE.

Digital Object Identifier 10.1109/TUFFC.2011.2055

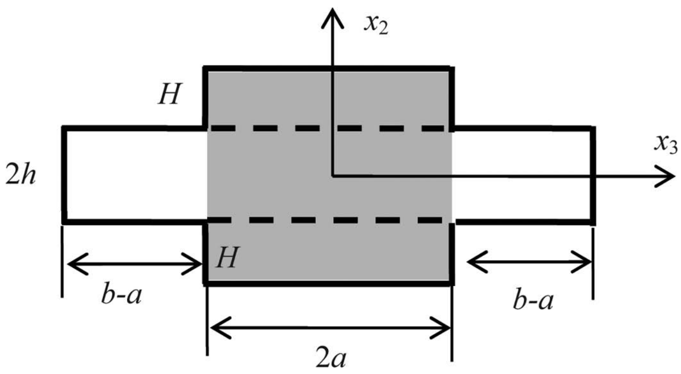

Fig. 1. A mesa resonator of AT-cut quartz.

plates of different cuts exhibit different anisotropies in coordinates normal and parallel to the plate surfaces. The widely used AT-cut quartz plate is a special case of rotated Y-cut quartz plates which are effectively monoclinic in the plate coordinate system [21]. Consider an AT-cut quartz mesa resonator made from a plate with stepped thickness as shown in Fig. 1. The plate is unbounded in the x_1 direction and does not vary along x_1. Fig. 1 shows a cross section. In the vertical (x_2) direction, we artificially divide the plate cross section into three rectangular regions at the two dotted lines and call them the top ($h < x_2 < h + H$), middle ($-h < x_2 < h$), and bottom ($-(h + H) < x_2 < -h$) regions, respectively. In the horizontal (x_3) direction, we call the thick shaded region ($|x_3| < a$) the inner region, and the unshaded thinner regions with $a < |x_3| < b$ the outer regions. Quartz has very weak piezoelectric coupling [21]. For free vibration frequency analysis, the small piezoelectric coupling can usually be neglected and an elastic analysis is sufficient. For monoclinic crystals, shear-horizontal (SH) or antiplane motions with only one displacement component $u_1(x_2, x_3, t)$ are allowed by the linear theory of anisotropic elasticity. The corresponding modes are TSh and TT modes as well as face-shear modes. SH motions in rotated Y-cut quartz are described by [4]

$$u_1 = u_1(x_2, x_3, t), \quad u_2 = u_3 = 0, \tag{1}$$

where $\mathbf{u}$ is the displacement vector. The nonzero components of the strain tensor $\mathbf{S}$ and the stress tensor $\mathbf{T}$ are

$$S_5 = 2S_{31} = u_{1,3}, \quad S_6 = 2S_{21} = u_{1,2}, \tag{2}$$

$$T_{31} = c_{55}u_{1,3} + c_{56}u_{1,2}, \quad T_{21} = c_{56}u_{1,3} + c_{66}u_{1,2}, \tag{3}$$

where $\mathbf{c}$ is the elastic stiffness tensor. The relevant equation of motion is

$$T_{21,2} + T_{31,3} = \rho \ddot{u}_1. \tag{4}$$

The equation to be satisfied by u_1 is obtained by substituting (3) into (4):

$$c_{66}u_{1,22} + c_{55}u_{1,33} + 2c_{56}u_{1,23} = \rho \ddot{u}_1. \tag{5}$$

These equations are valid in every rectangular region in Fig. 1. We will obtain expressions for the fields in each region and match them at the interfaces. We consider time-harmonic motions. All fields have the same $\exp(i\omega t)$ factor which will be dropped for simplicity. The boundary condition at the top of the inner region of the plate ($|x_3| < a$) is

$$T_{21}(x_3, h + H) = 0, \quad |x_3| < a. \tag{6}$$

The continuity conditions at the interface between the top and middle rectangular regions are

$$\begin{aligned} &u_1(x_3, h^-) = u_1(x_3, h^+), \quad |x_3| < a, \\ &T_{21}(x_3, h^-) = \begin{cases} T_{21}(x_3, h^+), & |x_3| < a, \\ 0, & a < |x_3| < b. \end{cases} \end{aligned} \tag{7}$$

The right edges of the top and middle rectangular regions are traction free, with

$$T_{31}(a, x_2) = 0, \quad h < |x_2| < h + H, \tag{8}$$

$$T_{31}(b, x_2) = 0, \quad |x_2| < h. \tag{9}$$

The plate in Fig. 1 is symmetric in both x_2 and x_3. For the applications we are considering, we are interested in modes that are symmetric in x_3 and antisymmetric in x_2. Because of symmetry and antisymmetry, the boundary and continuity conditions at the lower interface $x_2 = -h$, the bottom surface $x_2 = -(h + H)$, and the left edges will not be needed. For AT-cut quartz plates, $c_{55} = 68.81$, $c_{56} = 2.53$, and $c_{66} = 29.01 \times 10^9$ N/m^2 [21]. c_{56} is very small compared with c_{55} and c_{66}. Therefore, in the rest of this paper, we will make the usual approximation of neglecting the small c_{56} [22].

III. Fourier Series Solution

Consider free vibrations for which

$$u_1(x_2, x_3, t) = u_1(x_2, x_3)\exp(i\omega t). \tag{10}$$

We will obtain fields in the top and middle rectangular regions. Fields in the bottom rectangular region are not needed because of symmetry.

A. Fields in the Middle Region

The following solution can be constructed from standard separation of variables:

$$u_1 = B_0 \sin(\eta_0 x_2) + \sum_{m=1}^{\infty} B_m \sin(\eta_m x_2) \cos\frac{m\pi x_3}{b}, \tag{11}$$

where B_0 and B_m are undetermined constants, and

$$\eta_m^2 = \frac{\rho\omega^2}{c_{66}} - \frac{c_{55}}{c_{66}}\left(\frac{m\pi}{b}\right)^2 = \frac{\pi^2}{4h^2}\left[\frac{\omega^2}{\omega_s^2} - \frac{c_{55}}{c_{66}}\left(m\frac{2h}{b}\right)^2\right], \tag{12}$$
$$m = 0, 1, 2, 3, \ldots,$$

$$c_{66}B_0\eta_0\cos(\eta_0 h) + c_{66}\sum_{m=1}^{\infty} B_m\eta_m\cos(\eta_m h)\cos\frac{m\pi x_3}{b}$$
$$= \begin{cases} -c_{66}C_0\xi_0\sin(\xi_0 h) + c_{66}D_0\xi_0\cos(\xi_0 h) + c_{66}\sum_{m=1}^{\infty}[-C_m\xi_m\sin(\xi_m h) + D_m\xi_m\cos(\xi_m h)]\cos\frac{m\pi x_3}{a}, & |x_3| < a, \\ 0, & a < |x_3| < b. \end{cases} \quad (22)$$

$$\omega_s = \frac{\pi}{2h}\sqrt{\frac{c_{66}}{\rho}}. \quad (13)$$

Eq. (11) satisfies (5) and (9) when the small c_{56} is neglected. ω_s is the resonant frequency of the fundamental TSh mode in an unbounded quartz plate with a thickness of $2h$. For large m, η_m^2 as defined in (12) is negative. In that case, we can redefine

$$-\eta_m^2 = \frac{\pi^2}{4h^2}\left[\frac{\omega^2}{\omega_s^2} - \frac{c_{55}}{c_{66}}\left(m\frac{2h}{b}\right)^2\right], \quad m = 0,1,2,3,\ldots, \quad (14)$$

and, correspondingly, (11) becomes

$$u_1 = B_0\sinh(\eta_0 x_2) + \sum_{m=1}^{\infty} B_m\sinh(\eta_m x_2)\cos\frac{m\pi x_3}{b}. \quad (15)$$

In the following, we will formally use (11) and (12) and implement (14) and (15) in the computer code when needed. For resonator applications thin plates with small h/b are usually used; for these, (12) is the main situation. To apply the boundary and continuity conditions at the plate top and bottom, we need

$$T_{21} = c_{66}u_{1,2} = c_{66}B_0\eta_0\cos(\eta_0 x_2) + c_{66}\sum_{m=1}^{\infty} B_m\eta_m\cos(\eta_m x_2)\cos\frac{m\pi x_3}{b}. \quad (16)$$

B. Fields in the Top Region

We construct the following solution from separation of variables:

$$u_1 = C_0\cos(\xi_0 x_2) + D_0\sin(\xi_0 x_2) + \sum_{m=1}^{\infty}[C_m\cos(\xi_m x_2) + D_m\sin(\xi_m x_2)]\cos\frac{m\pi x_3}{a}, \quad (17)$$

where C_0, D_0, C_m, and D_m are undetermined constants, and

$$\xi_m^2 = \frac{\rho\omega^2}{c_{66}} - \frac{c_{55}}{c_{66}}\left(\frac{m\pi}{a}\right)^2 = \frac{\pi^2}{4h^2}\left[\frac{\omega^2}{\omega_s^2} - \frac{c_{55}}{c_{66}}\left(m\frac{2h}{a}\right)^2\right], \quad (18)$$
$$m = 0,1,2,3,\ldots.$$

Eq. (17) satisfies (5) and (8) when c_{56} is neglected. To apply boundary and continuity conditions, we need

$$T_{21} = c_{66}u_{1,2} = -c_{66}C_0\xi_0\sin(\xi_0 x_2) + c_{66}D_0\xi_0\cos(\xi_0 x_2) + c_{66}\sum_{m=1}^{\infty}[-C_m\xi_m\sin(\xi_m x_2) + D_m\xi_m\cos(\xi_m x_2)] \times \cos\frac{m\pi x_3}{a}. \quad (19)$$

IV. Boundary and Continuity Conditions

Substitution of (11), (16), (17), and (19) into (6) and (7) yields

$$-c_{66}C_0\xi_0\sin[\xi_0(h+H)] + c_{66}D_0\xi_0\cos[\xi_0(h+H)] + c_{66}\sum_{m=1}^{\infty}\{-C_m\xi_m\sin[\xi_m(h+H)] + D_m\xi_m\cos[\xi_m(h+H)]\}\cos\frac{m\pi x_3}{a} = 0, \quad |x_3| < a, \quad (20)$$

$$B_0\sin(\eta_0 h) + \sum_{m=1}^{\infty} B_m\sin(\eta_m h)\cos\frac{m\pi x_3}{b} = C_0\cos(\xi_0 h) + D_0\sin(\xi_0 h) + \sum_{m=1}^{\infty}[C_m\cos(\xi_m h) + D_m\sin(\xi_m h)]\cos\frac{m\pi x_3}{a}, \quad |x_3| < a, \quad (21)$$

and (22), see above.

We multiply both sides of (20) and (21) by $\cos n\pi x/a$ $(n = 0, 1, 2, \ldots)$ and integrate the resulting expression over $(-a, a)$, and multiply both sides of (22), see above, by $\cos n\pi x/b$ $(n = 0, 1, 2, \ldots)$ and integrate the resulting expression over $(-b, b)$. This leads to a system of linear homogeneous equations for the undetermined coefficients in the Fourier series, representing an eigenvalue problem. These equations are solved using a computer.

V. Numerical Results

As an example, we consider a mesa resonator with the following dimensions: $a = 5$ mm, $b = 8$ mm, $2h = 0.3$ mm, and $H = 0.08$ mm. The required material constants can be found in [21]. The modes we are interested in have slow variations in the x_3 direction, with no more than a few nodal points (zeros). Numerical tests show that to describe such a slow variation we do not need many terms in the series. The top region with $|x_3| < a$ is shorter than the middle region with $|x_3| < b$. Therefore, we use fewer terms for the top region than the middle region. A few TSh and TT modes can be found in the frequency range of interest. The mode we are most interested is the first trapped mode (transversely varying TSh) with the lowest frequency. Calculations show that when using 11 terms for the series of the middle region and 7 terms for the series of the top region, the frequency of the first mode is 2.264783×10^7 rad/s. When using 12 terms for the middle region and 8 terms for the top region, the frequency of the first mode is 2.264773×10^7 rad/s. The first 5 digits of the two frequencies are the same. This means that taking 12 terms and 8 terms is sufficient. In this case, the η_m^2 in (12) and the ξ_m^2 in (18) are both positive.

Fig. 2 shows the four lowest trapped modes of interest in order of increasing frequency. The displacement distributions of these modes at $x_2 = h$ are shown in Fig. 3. Twelve terms are used in the series for the middle region and 8 terms are used for the top region. $\omega_1 = 2.264773 \times 10^7$ rad/s, $\omega_2 = 2.302294 \times 10^7$ rad/s, $\omega_3 = 2.377118 \times 10^7$ rad/s, and $\omega_4 = 2.487805 \times 10^7$ rad/s. The modes in Fig. 2 are normalized in such a way that the maximal displacement at the plate top surface $x_2 = h + H$ is equal to one. The first mode is a transversely varying TSh mode. The others are TT modes. For all of these modes, the vibration is large in the inner region of the plate ($|x_3| < a$) and small in the outer regions, especially near the plate edges, where the vibration is essentially zero. This is the so-called energy trapping in mesa resonators. In the first TSh mode, the whole plate is vibrating in phase. The other TT modes all have nodal lines. Higher-order modes have more nodal lines. When modal lines are present, the charges on the electrodes (which are usually on the plate top and bottom) produced by the shear strain tend to cancel each other and thus reduce the capacitance of the resonator. This may be undesirable or desirable, depending on the specific application. We note that the first two modes agree with the pictures from experimental measurements shown in [18, Fig. 5].

Fig. 4 shows the effect of a, the length of the thick inner region, on the first trapped mode. The curves are for u_1 versus x_3 at $x_2 = h$. Calculations show that larger values of a are associated with lower frequencies because of the additional inertia. For the three modes shown, $\omega_1 = 2.267035 \times 10^7$ rad/s, 2.264773×10^7 rad/s, and 2.262611×10^7 rad/s, respectively. The vibration distribution follows a and is sensitive to a. A larger a has a wider vibration distribution. Numerical results show that the number of trapped modes depends on a and is very sensitive to a. The results are summarized in Table I.

Fig. 5 shows the effect of H on the first trapped mode. Numerical results show that larger values of H lead to

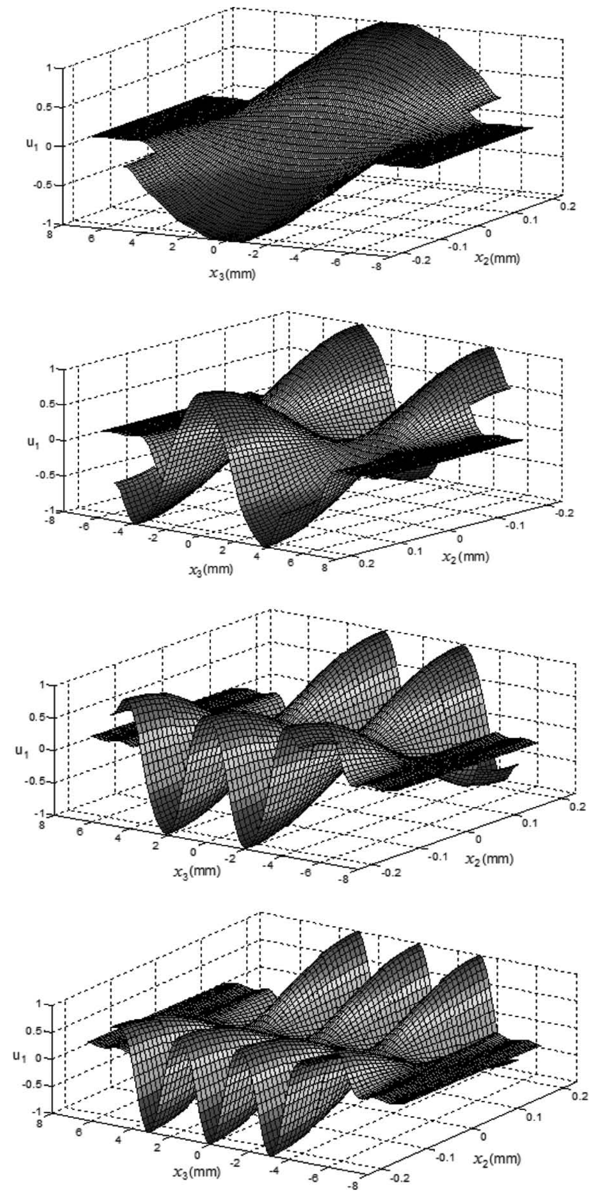

Fig. 2. The four lowest trapped modes.

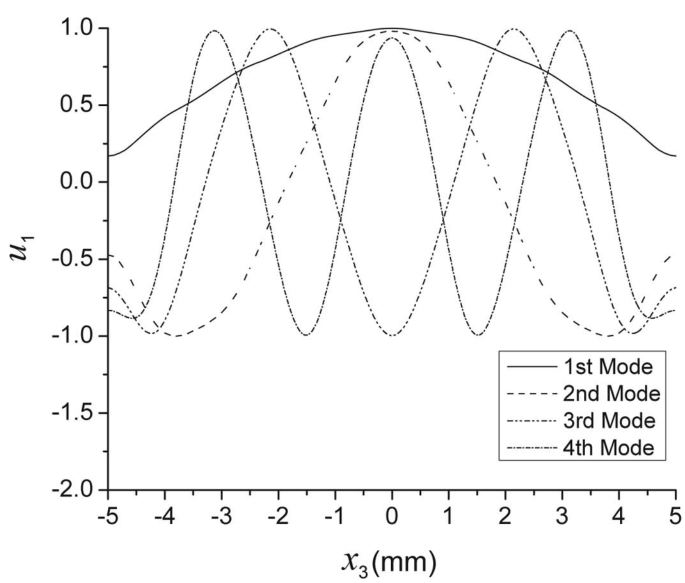

Fig. 3. u_1 versus x_3 at $x_2 = h$ for the four lowest modes.

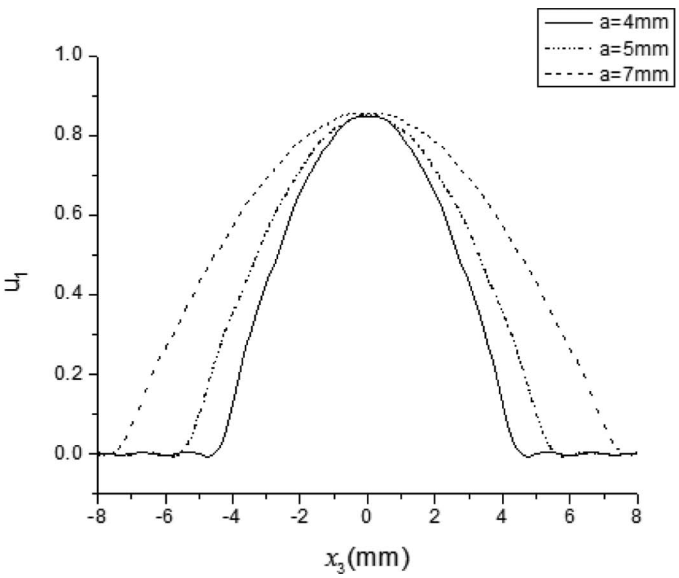

Fig. 4. Effect of a on the first mode.

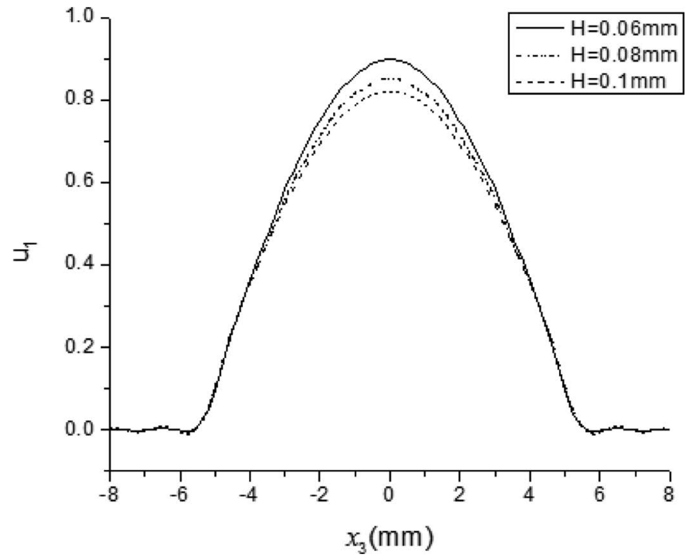

Fig. 5. Effect of H on the first mode.

TABLE I. Number of Trapped Modes Versus a.

a (mm)	N (number of modes)
0.6	1
0.7	2
1	2
2	3
3	5
4	6
5	8
6	9
7	11

lower frequencies. For the three modes shown, $\omega_1 = 2.479719 \times 10^7$ rad/s, 2.264773×10^7 rad/s and 2.084216×10^7 rad/s. The mode shape is not very sensitive to H. The width of the vibration distribution is essentially unaffected by H. For larger values of H, u_3 at $x_2 = h$ becomes slightly smaller.

VI. Conclusion

For SH motions of a mesa resonator with stepped thickness, a Fourier series solution can be obtained by dividing the resonator into several regions and matching the series in different regions at the interfaces. The solution obtained is able to show the basic behaviors of a mesa resonator. A mesa resonator can produce energy trapping of TSh and TT modes. The trapping of the first TSh mode is very sensitive to the length of the thick inner region, but not sensitive to the thickness of the inner region. It is expected that the method used in this paper can also be used to analyze resonators with other stepped thickness configurations, e.g., the so-called inverted mesa, for which the inner region is thinner.

References

[1] I. Koga, "Thickness vibrations of piezoelectric oscillating crystals," *Physics*, vol. 3, no. 2, pp. 70–80, 1932.

[2] H. F. Tiersten, "Thickness vibrations of piezoelectric plates," *J. Acoust. Soc. Am.*, vol. 35, no. 1, pp. 53–58, 1963.

[3] H. F. Tiersten, "A corrected modal representation of thickness vibrations in quartz plates and its influence on the transversely varying case," *IEEE Trans. Ultrason. Ferroelectr. Freq. Control*, vol. 50, no. 11, pp. 1436–1443, 2003.

[4] R. D. Mindlin, "Thickness-twist vibrations of an infinite, monoclinic, crystal plate," *Int. J. Solids Struct.*, vol. 1, no. 2, pp. 141–145, 1965.

[5] Z. T. Yang, Y. T. Hu, and J. S. Yang, "Effect of mass layer stiffness on propagation of thickness-twist waves in rotated y-cut quartz crystal plates," *Ultrasonics*, vol. 49, no. 4–5, pp. 401–403, 2009.

[6] R. D. Mindlin and P. C. Y. Lee, "Thickness-shear and flexural vibrations of partially plated, crystal plates," *Int. J. Solids Struct.*, vol. 2, no. 1, pp. 125–139, 1966.

[7] J. S. Yang and J. A. Kosinski, "Effects of piezoelectric coupling on energy trapping of thickness-shear modes," *IEEE Trans. Ultrason. Ferroelectr. Freq. Control*, vol. 51, no. 9, pp. 1047–1049, 2004.

[8] H. F. Tiersten and R. C. Smyth, "Analysis of contoured crystal resonators operating in overtones of coupled thickness shear and thickness twist," *J. Acoust. Soc. Am.*, vol. 65, no. 6, pp. 1455–1460, 1979.

[9] H. F. Tiersten and D. S. Stevens, "An analysis of nonlinear resonance in contoured-quartz resonators," *J. Acoust. Soc. Am.*, vol. 80, no. 4, pp. 1122–1132, 1986.

[10] M. Onoe and K. Okada, "Analysis of contoured piezoelectric resonators vibrating in thickness-twist modes," in *Proc. 23rd Annual Frequency Control Symp.*, 1969, pp. 26–38.

[11] B. K. Sinha, "Doubly rotated contoured quartz crystal resonators," *IEEE Trans. Ultrason. Ferroelectr. Freq. Control*, vol. 48, no. 5, pp. 1162–1180, 2001.

[12] F. Shen, S. J. O'Shea, K. H. Lee, P. Lu, and T. Y. Ng, "Frequency interference between two mesa-shaped quartz crystal microbalance," *IEEE Trans. Ultrason. Ferroelectr. Freq. Control*, vol. 50, no. 6, pp. 668–675, 2003.

[13] A. Ishizaki, H. Sekimoto, D. Tajima, and Y. Watanabe, "Analysis of spurious vibrations in mesa-shaped AT-cut quartz plates," in *Proc. IEEE Ultrasonics Symp.*, 1995, pp. 913–916.

[14] S. Goka, H. Sekimoto, and Y. Watanabe, "Experimental study of vibrations of mesa-shaped AT-cut quartz plates," in *Proc. IEEE Int. Frequency Control Symp.*, 1999, pp. 441–444.

[15] S. Goka, H. Sekimoto, and Y. Watanabe, "Decoupling effect of stepped mesa structures on spurious vibrations of AT-cut quartz plates," in *Proc. IEEE Int. Frequency Control Symp.*, 2000, pp. 397–400.

[16] H. Sekimoto, S. Goka, and Y. Watanabe, "Analysis of 3-D vibrations of rectangular AT-cut quartz plates with a bi-mesa structure," *IEEE Trans. Ultrason. Ferroelectr. Freq. Control*, vol. 48, no. 5, pp. 1302–1307, 2001.

[17] S. Goka, K. Tamura, H. Sekimoto, Y. Watanabe, and T. Sato, "Decoupling effect of multi-stepped bi-mesa AT-cut quartz resonators," in *Proc. IEEE Int. Frequency Control Symp.*, 2003, pp. 694–697.

[18] Y. Watanabe, S. Goka, T. Sato, and H. Sekimoto, "Non-scanning measurements for determining in-plane mode shapes in piezoelectric devices with polished surfaces," in *Proc. IEEE Int. Frequency Control Symp.*, 2003, pp. 753–756.

[19] S. Goka, Y. Mase, H. Sekimoto, Y. Watanabe, and T. Sato, "Experimental study of mode-coupling strength of AT-cut quartz resonators with high mesa step height," in *Proc. IEEE Int. Frequency Control Symp.*, 2004, pp. 621–624.

[20] S. Goka, Y. Mase, H. Sekimoto, and Y. Watanabe, "Calculation of bi-mesa structures suitable for mounting," in Proc. *IEEE Int. Frequency Control Symp.*, 2006, pp. 205–208.

[21] H. F. Tiersten, *Linear Piezoelectric Plate Vibrations*, New York, NY: Plenum, 1969.

[22] H. F. Tiersten, "Analysis of trapped-energy resonators operating in overtones of coupled thickness shear and thickness twist," *J. Acoust. Soc. Am.*, vol. 59, no. 4, pp. 879–888, 1976.

Authors' photographs and biographies were unavailable at time of publication.